Journal of Alloys and Compounds 509 (2011) 1424–1429

Contents lists available at ScienceDirect

Journal of Alloys and Compounds

journal homepage: www.elsevier.com/locate/jallcom

Magnetic characterization of polycrystalline $NdFeAsO_{0.88}F_{0.12}$ oxypnictide superconductor

Y. Ding[a], Y. Sun[a], X.D. Wang[a], Z.X. Shi[a,*], Z.A. Ren[b], J. Yang[b], W. Lu[b]

[a] Department of Physics, Southeast University, Nanjing 211189, PR China
[b] Institute of Physics and Beijing National Laboratory for Condensed Matter Physics, Chinese Academy of Science, Beijing 100190, PR China

ARTICLE INFO

Article history:
Received 24 August 2010
Received in revised form 3 November 2010
Accepted 5 November 2010
Available online 12 November 2010

PACS:
74.70.Xa
74.25.Ha
74.25.N–

Keywords:
High-T_c superconductors
Magnetization
Magnetic measurements
Granularity

ABSTRACT

The superconducting properties of polycrystalline $NdFeAsO_{0.88}F_{0.12}$ oxypnictide were studied by both DC and AC magnetization measurements. The zero-field cooled (ZFC) magnetic susceptibility, $\chi(T)$, measured under the magnetic field of 0.5 T shows a dramatic decrease at about 11 K. The imaginary component of the first harmonics of the AC magnetic susceptibility, $\chi''(T)$, increases with the increasing DC field H_{dc} below 11 K. These results indicate the onset of robust intergranular superconductivity at low temperatures. The magnetic hysteresis loops show an anomalous double central peak effect at low temperatures, with one peak at positive fields in decreasing positive external fields. This phenomenon suggests the granular character of this system. The paramagnetism of Nd^{3+} ions tilts the magnetic hysteresis loops and broadens the hysteresis width ΔM. After correction for the paramagnetism, the temperature and field dependence of the average magnetization critical current density J_{cm} was obtained. The related mechanism was discussed.

1. Introduction

The recent discovery of superconductivity at 26 K in the iron oxypnictide LaFeAs(O, F) [1] has stimulated great interests among condensed-matter physics community. Tremendous work was carried out, leading to the emergence of novel iron-based superconductor families with different crystal structures: 1 1 1 1 (REFeAs(O, F)), 1 2 2 ((Ba, K)Fe_2As_2) [2], 1 1 1 (LiFeAs) [3] and 1 1 (Fe(Se, Te)) [4]. The REFeAs(O, F) superconductors, in which T_c is over 50 K when La is replaced by Sm [5], Gd [6] or Tb [7], crystallize in the tetragonal *P*4/*nmm* space group with two formula units per unit cell. The crystal structure consists of alternating RE–O and Fe–As layers stacked along the *c* axis. Since magnetic elements such as Fe and rare earths exist in this system, relevant questions have been raised about the relationship between magnetism and superconductivity. Muon spin rotation (μSR), neutron, and Mossbauer measurements [8,9] on undoped LaFeAsO have revealed commensurate spin density wave (SDW) ordering of the Fe moments below $T_N = 135$ K with amplitude of $0.35\mu_B$. Superconductivity can be induced from the magnetically ordered parent compound by carrier doping or external or internal pressure. Some measurements suggest that the magnetic order is rapidly suppressed upon doping and the maximum T_c is achieved just as static magnetism disappears [8,10]. Tarantini et al. excluded the long-range antiferromagnetic order in the superconducting $NdFeAsO_{0.94}F_{0.06}$ [11], consistent with neutron measurements down to 1.5 K [12]. However, μSR results suggest that long range magnetic ordering may exist below 2.4 K for Nd-1 1 1 1 and below 4 K for Ce-1 1 1 1 compounds [13]. Drew et al. detected magnetic fluctuations [14] and static magnetism [15] coexisting in the $SmFeAsO_{1-x}F_x$ by μSR, and Ryan et al. detected the coexistence of long-ranged magnetic order and superconductivity in $SmFeAsO_{1-x}F_x$ by using neutron diffraction [16]. The coexistence of magnetism and superconductivity, and the role played by magnetism in the basic superconducting mechanism need to be further investigated both theoretically and experimentally.

Besides the studies related to the superconducting mechanism, it is also necessary to study the vortex pinning properties, which are of great importance on potential applications. Recent reports have shown the modified electromagnetic behavior [11,17,18] by magnetism of rare earth ions and the granularity [19–21] in the 1 1 1 1 system. Our previous work [22] shows that weak links and strong links coexist in the Nd-1 1 1 1 system, and the strong links persist up to 9 T. In this paper, both DC and AC magnetization measurements were performed to study the vortex pinning properties of the $NdFeAsO_{0.88}F_{0.12}$ superconductor. The influence of

* Corresponding author.
E-mail address: zxshi@seu.edu.cn (Z.X. Shi).

0925-8388/$ – see front matter © 2010 Elsevier B.V. All rights reserved.
doi:10.1016/j.jallcom.2010.11.050

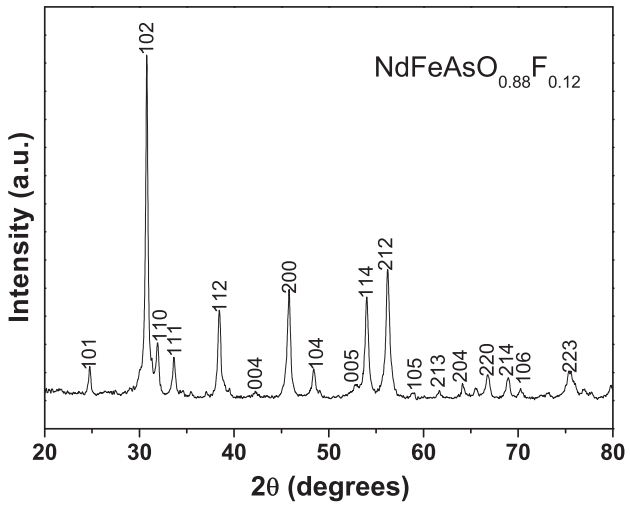

Fig. 1. X-ray powder diffraction patterns of the $NdFeAsO_{0.88}F_{0.12}$ sample.

paramagnetism of Nd^{3+} ions on the magnetization critical current density was also investigated.

2. Experimental

The polycrystalline $NdFeAsO_{1-x}F_x$ superconducting sample was prepared directly by a high-pressure method similar to [23]. The starting materials were mixed according to the nominal stoichiometric ratio of $NdFeAsO_{0.88}F_{0.12}$, then ground thoroughly and pressed into pellets. The pellets were sealed in boron nitride crucibles and sintered under 6 GPa in a high-pressure synthesis apparatus at the temperature of 1250 °C for 2 h. The sample had the dimensions of 1.16 mm × 1.88 mm × 4.50 mm, a mass of 58 mg and is therefore about 82% of the theoretical density (7.21 g/cm^3).

The crystal structure of the sample was characterized by powder X-ray diffraction (XRD) on an MXP18A-HF–type diffractometer with Cu-Kα radiation from 2Θ = 20–80 ° with a step-scan of 0.01 °. As shown in Fig. 1, all main peaks can be well indexed based on the ZrCuSiAs tetragonal structure, confirming the formation of NdFeAs(O, F) phase. No impurity peak was observed.

DC magnetization $M(T)$ and $M(H)$ measurements were performed using a vibrating sample magnetometer (VSM) of a Quantum Design PPMS. Magnetic critical current densities J_{cm} were estimated using the Bean model from the $M(H)$ hysteresis loops (MHLs). By using the PPMS equipped with an AC susceptometer, the first harmonics of the AC magnetic susceptibility as a function of the temperature were measured at various frequencies, ν, AC magnetic field amplitudes, h_{ac}, and DC fields, H_{dc}, which were parallel to the AC field. Before each measurement, the magnetic field was oscillated to reduce the residual field and the sample was warmed up to 60 K to fully expel the flux trapped inside. Sufficient waiting time was adopted to ensure the thermal homogeneity. During both DC and AC measurements, the magnetic fields were applied along the longest dimension of the sample.

3. Results and discussion

3.1. The DC magnetic susceptibilities

The DC magnetic susceptibilities $\chi(T)$ were measured by zero-field cooling (ZFC) and field cooling (FC) under 1.5 mT and 0.5 T. Fig. 2(a) shows the $\chi(T)$ curves measured under 1.5 mT. The sharp diamagnetic superconducting transition indicates good sample quality. After demagnetization correction, the superconducting shielding volume fraction was estimated to be 78%, confirming bulk superconductivity. The transition temperature T_c determined by the onset of diamagnetic signal is about 50 K. Fig. 2(b) shows the $\chi(T)$ curves measured under 0.5 T. The magnetic fields suppressed the superconducting diamagnetism, and most part of the ZFC curve became positive due to the strong paramagnetic background. It is also noted that the ZFC curve shows a sharp decrease and a broad shoulder at about 11 K. Similar behavior was reported by several groups in Nd [11], Sm [18] and Pr [24] 1111 superconductors. To investigate the origin of this behavior, the paramagnetic background was evaluated and subtracted from the total susceptibilities. Assuming that the paramagnetic magnetic moments of the Nd^{3+} ions do not interact with each other, the paramagnetic magnetization is expected to be given by

$$M_{pm} = M_0 B_J\left(\frac{g\mu_B JB}{k_B(T+\Theta)}\right) \quad (1)$$

where g is the Lande factor, μ_B is the Bohr magneton, k_B is the Boltzmann constant, $B_J(x)$ is the Brillouin function and $M_0 = NgJ\mu_B$, N is the number of Nd ions per unit volume. A phenomenological parameters Θ was introduced because the electric crystal field (CEF) acting on Nd 4f electrons splits and mixes the degenerated $|JM_J\rangle$ states resulting in, for $g\mu_B JB/k_B T \ll 1$, the modification of the Curie form $\chi = C/T$ to the Curie–Weiss law, $\chi = C/(T+\Theta)$ [25]. According to the Russell–Saunders coupling model the ground state term of the Nd^{3+} ion is $^4I_{9/2}$ (J = 9/2).

The $M(T)$ curve measured from 50 to 300 K under 0.75 T was plotted in Fig. 2(c), showing the Curie–Weiss behavior similar to reference [26]. The paramagnetic background of total magnetization from 5 to 50 K was obtained by fitting the measured $M(T)$ curve using Eq. (1) with parameter Θ = 16 K and $M_0 V = 3.26 \times 10^{-3}$ A m^2, where V is the sample volume. The density of Nd^{3+} ions as obtained is 1.22×10^{28} m^{-3}, agreed with the actual value of 1.09×10^{28} m^{-3}. The 0.5 T paramagnetic background-subtracted $\chi(T)$ curves are presented in Fig. 2(d). The $\chi(T)$ curves show negative values below the superconducting onset temperature, indicating the diamagnetic effect. The shoulder in the ZFC $\chi(T)$ curve disappeared. The FC $\chi(T)$ curve in Fig. 2(d) increases below 15 K. This may be caused by the underestimating of the paramagnetic component at low temperature, where the M_{pm} value deviates from Eq. (1). The dramatic decrease on ZFC 0.5 T $\chi(T)$ curve at about 11 K is not likely caused by small amounts of magnetic impurities, which were not detected by XRD analysis. The possible impurities in Nd-1 1 1 1 sample are Nd_2O_3, NdOF, Fe_2O_3, FeF_2, Fe–As and Nd–Fe systems. Nd_2O_3 and NdOF are paramagnetic at low temperatures [11,27], small amounts of antiferromagnetic FeF_2, Fe_2As, FeAs and $FeAs_2$ with T_N of 78 [28,29], 353, 77 and <5 K [30], respectively, should not have decisive effect on $M(T)$ behavior from 5 to 50 K. The existence of ferromagnetic Fe_2O_3 and Nd–Fe systems with Curie temperatures of more than 273 K [31] can be excluded by $M(H)$ measurements presented later. In a previous report [24], the decrease in $\chi(T)$ was explained by the onset of intergranular superconductivity. AC magnetic susceptibilities measurements were performed to further investigate this system, since the onset of superconductivity will cause a peak in the imaginary part of the χ'', representing losses due to field penetration.

3.2. The AC magnetic susceptibilities

Fig. 3(a) shows the AC magnetic susceptibilities χ' and χ'' as function of temperature at frequencies of 100 Hz, 500 Hz and 1 kHz, for DC magnetic fields $\mu_0 H_{dc}$ = 0.5 T and the AC magnetic field $\mu_0 h_{ac}$ = 0.8 mT. As the frequency decreases, the transition temperature shifts to lower values and the peak height in χ'' decreases as it moves to lower temperatures. Fig. 3(b) shows the $\chi'(T)$ and $\chi''(T)$ curves measured at the fixed frequency ν = 500 Hz, $\mu_0 h_{ac}$ = 1.6 mT and at various $\mu_0 H_{dc}$ = 5 mT, 15 mT, 50 mT, 0.5 T and 0.75 T. As the DC fields increase, the transition in $\chi'(T)$ and $\chi''(T)$ becomes broad and the peak height in χ'' decreases as it moves to lower temperature. These features are similar to that of high-temperature superconductors [32,33] and can be explained by flux creep and the temperature dependence of shielding currents [34]. It is noted that in Fig. 3(a), χ'' increased at low temperatures, and in Fig. 3(b), a weak peak in χ'' at about 11 K emerges when $\mu_0 H_{dc}$ = 50 mT and the peak seems to move below 5 K when $\mu_0 H_{dc}$ reaches 0.5 T. These features may be explained by the onset of intergranular

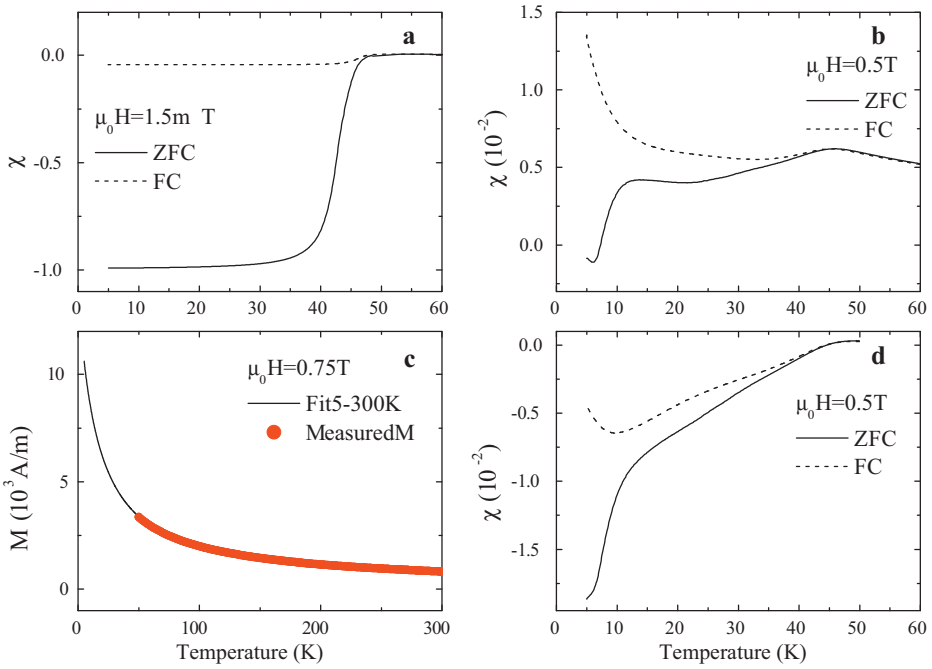

Fig. 2. The ZFC and FC $\chi(T)$ curves under (a) 1.5 mT, (b) 0.5 T, (c) dots indicate the $M(T)$ curve measured from 50 to 300 K under 0.75 T. Solid line represents the paramagnetic magnetization calculated from Eq. (1). (d) The ZFC and FC $\chi(T)$ curves under 0.5 T after subtracting the paramagnetic component.

superconductivity corresponding to the sharp dropping in DC $\chi(T)$ at about 11 K as shown in Fig. 3(d). The fact that the increase in χ'' around 11 K in Fig. 3(a) is not show frequency-dependent may be due to very weak flux creep at low temperatures. It is worth mention that Polichetti et al.'s results [35] on $LaFeAsO_{0.92}F_{0.08}$ show that the onset of intergranular superconductivity caused a step-like $\chi'(T)$ and a dissipation peak on $\chi''(T)$ in low temperature with larger area than the dissipation peak due to intragranular component. The temperature corresponding to the crossover between a behavior mainly governed by intergranular and intergranular components, T_g, was determined. However, no low-temperature dissipation peak or T_g was observed on $\chi''(T)$ under $\mu_0 H_{dc} = 5$ mT and 15 mT here in Fig. 3(b). This can be explained by better connectivity among grains in Nd-1 1 1 1 system as reported in Refs. [20,21], thus higher DC fields are required to suppress the intergranular currents and separate the intergranular and intragranular components.

In addition, if the decrease in $\chi(T)$ results from the onset of intergranular superconductivity, then this decrease should correspond to an increase of the irreversible magnetization thus a broadening of the magnetic hysteresis loops (MHLs). The MHLs were measured and studied below.

3.3. Magnetic hysteresis loops

Fig. 4(a) shows the MHLs of the sample up to 1.5 T at several temperatures from 5 K to 25 K. The MHLs were shifted to higher value by a paramagnetic background caused by Nd^{3+} ions, resulting in a crossover of MHLs at different temperatures in the field range of 0.5 T to 1 T. This behavior was also observed in other reports

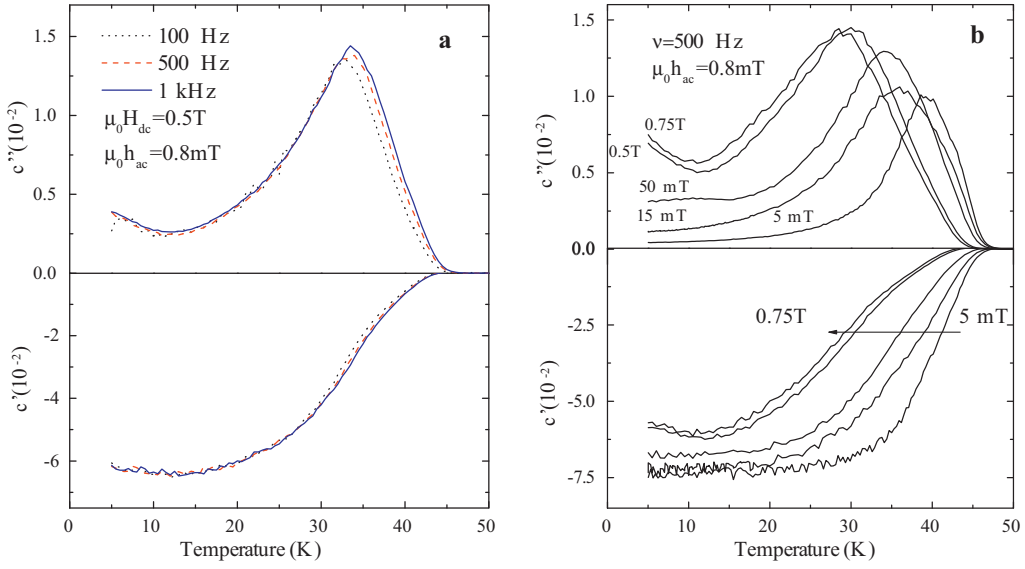

Fig. 3. (a) AC magnetic susceptibilities $\chi'(T)$ and $\chi''(T)$ at frequencies of 100 Hz, 500 Hz and 1 kHz, for $\mu_0 H_{dc} = 0.5$ T and $\mu_0 h_{ac} = 0.8$ mT. (b) The $\chi'(T)$ and $\chi''(T)$ curves measured at the fixed frequency $\nu = 500$ Hz, $\mu_0 h_{ac} = 1.6$ mT and at $\mu_0 H_{dc} = 5$ mT, 15 mT, 50 mT, 0.5 T and 0.75 T.

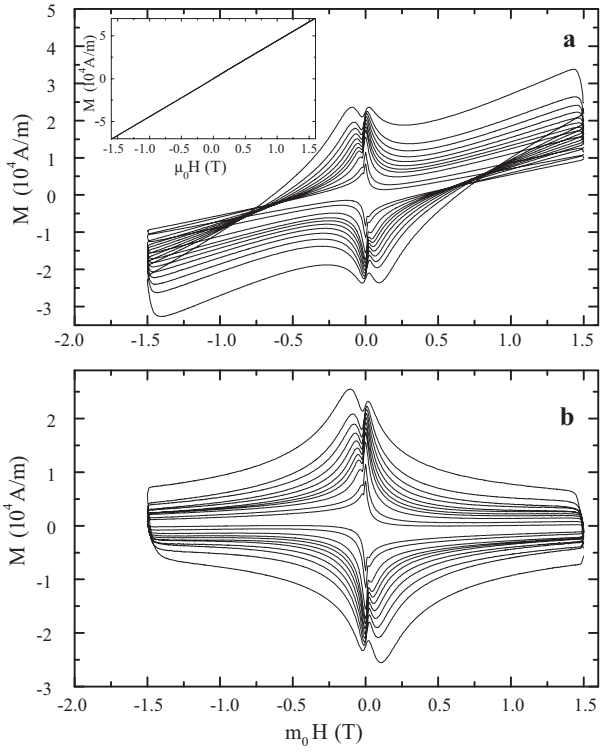

Fig. 4. (a) Magnetic hysteresis loops measured at 5, 7, 8, 9, 10, 11, 12, 13, 15, 20 and 25 K. Inset shows the $M(H)$ curve measured at 53 K up to 1.5 T. (b) Magnetic hysteresis loops after subtracting M_{pm} at 5–25 K.

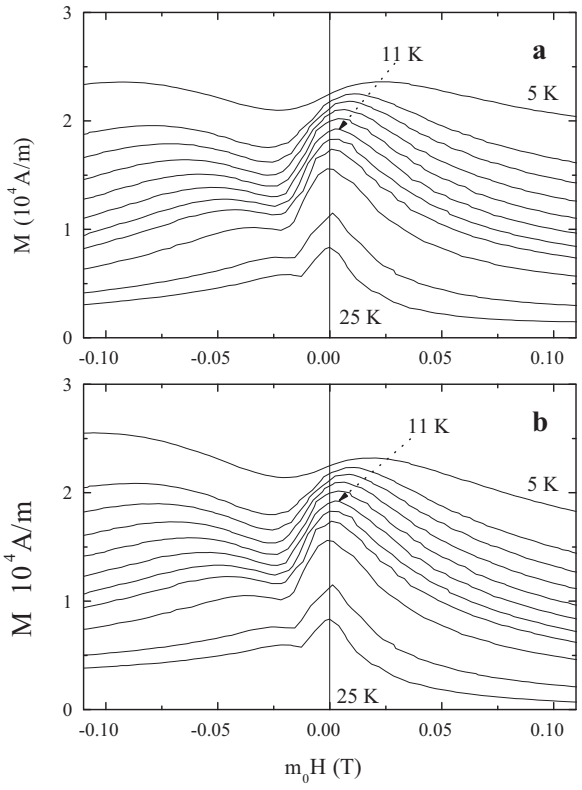

Fig. 5. (a) and (b) show the magnifications of the central peaks of MHLs in Fig. 4 before and after subtracting M_{pm}, respectively.

[17,26]. The magnetization $M(H)$ not masked by superconductivity was measured at 53 K up to 9 T (only to 1.5 T was shown in the inset of Fig. 4(a). No hysteresis or saturation was observed, thus the existence of magnetic impurities can be excluded.

The experimentally measured magnetization may contain two components: irreversible superconducting magnetization M_{sc}, the paramagnetic magnetization M_{pm} of Nd^{3+} ions.

$$M = M_{sc} + M_{pm} \tag{2}$$

$M_0V = 2.55 \times 10^{-3}$ A m^2 of the sample was determined by fitting the $M(H, 53\,K)$ curve using Eq. (1) with $\Theta = 0$ K for simplicity. The paramagnetic background of total MHLs measured at 5–25 K was then calculated using Eq. (1) with parameter $\Theta = 7$–9 K. The MHLs after subtracting M_{pm} were obtained and are shown in Fig. 4(b). It is noted that the MHLs show a double-peak effect, which was also observed in $NdFeAsO_{1-\delta}$ system [19] and high temperature superconductors [36]. The peaks in the second quadrant of the graph originate from bulk superconductivity with a regular temperature dependence. The peaks near $\mu_0 H = 0$ T are caused by granular superconductivity. The magnifications of the central peaks are shown in Fig. 5. Before and after paramagnetic correction, the granularity peaks, B_{pc}, are located at $\mu_0 H = 0$ T at 25–12 K, but shift to the first quadrant below 11 K. Similar behaviors were observed in silver-sheathed (Pb, Bi)$_2$Sr$_2$Ca$_2$Cu$_3$O$_{10+\delta}$ (Bi-2223) tapes [37–40] and model samples [41]. It was learned that the intergranular currents are responsible for the positive peak position. At low temperatures, the local field between grains, B_i, is reduced by the grain stray fields [37] and grain demagnetizing effect [38], leading to the experimentally observed situation that B_i is apparently ahead of the external field, B_e, and consequently $B_{pc} > 0$. This phenomenon confirms the granular nature in the oxypnictide superconductors [19–21]. Systematic studies on series of polycrystals and single crystals are needed to show whether the onset of intergranular superconductivity around 11 K is caused by extrinsic properties, e.g., local areas with better connectivity [19], or intrinsic properties, e.g., the decrease of superconducting anisotropy at low temperatures due to increased interlayer coupling or possible multigap effects [42].

3.4. Effect of paramagnetism on J_c

Because the distribution of the flux density in the sample during the increasing B^- and during the decreasing B^+ field process at the same applied field is different, the paramagnetic magnetization during the increasing field process M^-_{pm} and during the decreasing field process M^+_{pm} should be different as well. The Bean critical state model leads to the following expressions for the magnetization in the decreasing M^+ and in the increasing M^- field branches:

$$M^+ = \frac{\Delta M_{sc}}{2} + \left\langle M^+_{pm} \right\rangle \tag{3}$$

$$M^- = \frac{\Delta M_{sc}}{2} + \left\langle M^-_{pm} \right\rangle \tag{4}$$

where $\Delta M_{sc} = M^+_{sc} - M^-_{sc}$ is the magnetic hysteresis if there is no paramagnetic contribution, and $\left\langle M^\pm_{pm} \right\rangle$ is the spatial average of $M^\pm_{pm}$, respectively. From Eqs. (3) and (4) the width of the experimentally measured magnetic hysteresis ΔM should be:

$$\Delta M = \Delta M_{sc} + \Delta M_{pm} \tag{5}$$

where $\Delta M_{pm} = \left\langle M^+_{pm} \right\rangle - \left\langle M^-_{pm} \right\rangle$. Considering a fully penetrated infinitely long slab of thickness d along the x axis and infinite in the yz plane with the magnetic field H parallel to the z axis, and using the simple Bean critical state model with Eq. (2), the field dependence of ΔM_{pm} can be deduced as [43]:

$$\Delta M_{pm}(H) = \left\langle M^+_{pm} \right\rangle - \left\langle M^-_{pm} \right\rangle = M_0 \left(\left\langle B_J(\eta^+) \right\rangle - \left\langle B_J(\eta^-) \right\rangle \right) \tag{6}$$

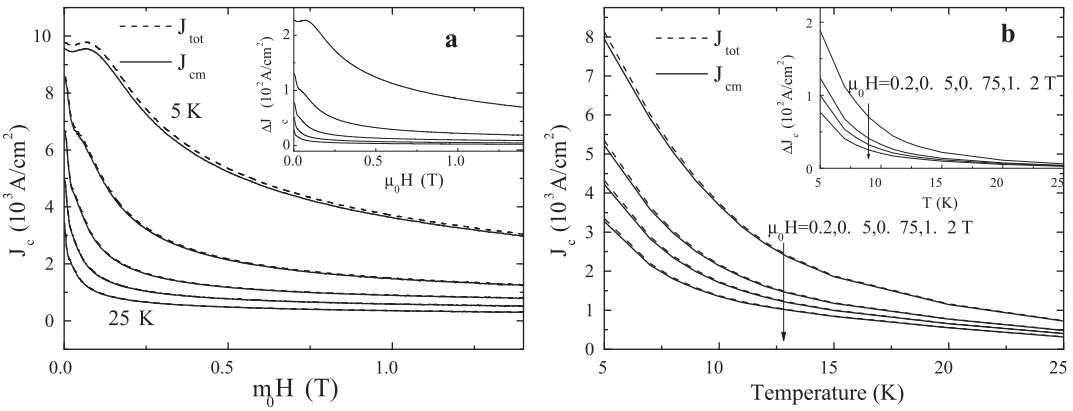

Fig. 6. (a) Comparison of $J_{tot}(H)$ and $J_{cm}(H)$ up to 1.4 T at 5, 10, 15, 20 and 25 K. Inset shows the field dependence of $\Delta J_c = J_{tot} - J_{cm}$ correspondingly. (b) Comparison of $J_{tot}(H)$ and $J_{cm}(H)$ at 5–25 K under 0.2, 0.5, 0.75 and 1.2 T. Inset shows the temperature dependence of $\Delta J_c = J_{tot} - J_{cm}$ correspondingly.

where $\eta = g\mu_B B^{\pm}/k_B(T+\Theta)$, B^- and B^+ is the flux density in the sample during the increasing field and during the decreasing field process respectively, and $\langle B_J(\eta^{\pm})\rangle$ is the spatial average of $B_J(\eta^{\pm})$.

As can be seen from Eq. (5), the experimentally measured magnetic hysteresis ΔM can be broadened by paramagnetism. Therefore, the total magnetic critical current density $J_{tot} = 20\Delta M/a(1 - a/3b)$ deviates from the average critical current density $J_{cm} = 20\Delta M_{sc}/a(1 - a/3b)$ due to this paramagnetic effect. Here a and b are the thickness and the width of the sample (only average J_{cm} can be derived from ΔM because the distribution of the current loop sizes is unknown). The field dependence of J_{tot} and J_{cm} at 5, 10, 15, 20 and 25 K are plotted in Fig. 6(a) for comparison. The paramagnetic component, $\Delta J_{cm} = J_{tot} - J_{cm}$, decreases monotonically with applied field as shown in the inset of Fig. 6(a). Fig. 6(b) shows the temperature dependence of J_{tot} and J_{cm} at 0.2 T, 0.5 T, 0.75 T and 1.2 T. The inset of Fig. 6(b) shows that ΔJ_{cm} decreases quickly with increasing temperature. In Fig. 6, it is obvious that J_{tot} is larger than J_{cm} at 5 K. However in high field and high temperature, ΔJ_{cm} can be neglected, thus J_{cm} can be well approximated by J_{tot}. The reason is that in the high field and high temperature region, magnetic hysteresis decreases quickly due to weak pinning, so the distribution of the flux density in the sample during the increasing B^- and during the decreasing B^+ field process at the same applied field is very close, resulting in much less difference between M_{pm}^- and M_{pm}^+.

4. Conclusions

In summary, the superconducting properties of the iron-based superconductor $NdFeAsO_{0.88}F_{0.12}$ was studied by means of both DC and AC magnetization measurements. The dramatic decrease in $\chi(T)$ curves under 0.5 T and the increase in $\chi''(T)$ at low temperatures suggest the onset of robust intergranular superconductivity. The double central peak effect and the positive central peaks in MHLs below 11 K confirm the granular nature of this system. The paramagnetism of Nd^{3+} ions tilted the magnetic hysteresis loops and broadened the hysteresis width, thus increasing the critical current density J_{tot} derived directly from MHLs at low temperatures and low fields.

Acknowledgments

This work was supported by the Scientific Research Foundation of Graduate School of Southeast University (Grant No. YBJJ0933), by the Natural Science Foundation of China (NSFC, Grant No. 10804127), by the Cyanine-Project Foundation of Jiangsu Province of China (Grant No. 1107020060) and by the Foundation for Climax Talents Plan in Six-Big Fields of Jiangsu Province of China (Grant No. 1107020070).

References

[1] Y. Kamihara, T. Watanabe, M. Hirano, H. Hosono, J. Am. Chem. Soc. 130 (2008) 3296.
[2] M. Rotter, M. Tegel, D. Johrendt, I. Schellenberg, W. Hermes, R. Pottgen, Phys. Rev. B 78 (2008), 020503 (R).
[3] X.C. Wang, Q.Q. Liu, Y.X. Lv, W.B. Gao, L.X. Yang, R.C. Yu, F.Y. Li, C.Q. Jin, Solid State Commun. 148 (2008) 538–540.
[4] F.C. Hsu, et al., Proc. Natl. Acad. Sci. U.S.A. 105 (2008) 14262.
[5] Z.A. Ren, et al., Chin. Phys. Lett. 25 (2008) 2215.
[6] C. Wang, et al., EPL 83 (2008) 67006, doi:10.1209/0295-5075/83/67006.
[7] L.J. Li, Y.K. Li, Z. Ren, Y.K. Luo, X. Lin, M. He, Q. Tao, Z.W. Zhu, G.H. Cao, Z.A. Xu, Phys. Rev. B 78 (2008) 132506.
[8] C. Cruz, et al., Nature 453 (2008) 899–902.
[9] H.H. Klauss, et al., Phys. Rev. Lett. 101 (2008) 077005.
[10] R.H. Liu, et al., Phys. Rev. Lett. 101 (2008) 087001.
[11] C. Tarantini, A. Gurevich, D.C. Larbalestier, Z.A. Ren, X.L. Dong, W. Lu, Z.X. Zhao, Phys. Rev. B 78 (2008) 184501.
[12] Y. Qiu, Wei Bao, Q. Huang, T. Yildirim, J.M. Simmons, M.A. Green, J.W. Lynn, Y.C. Gasparovic, J. Li, T. Wu, G Wu, X.H. Chen, Phys. Rev. Lett. 101 (2008) 257002.
[13] J.P. Carlo, et al., Phys. Rev. Lett. 102 (2009) 087001.
[14] A.J. Drew, et al., Phys. Rev. Lett. 101 (2008) 097010.
[15] A.J. Drew, et al., Nat. Mater. 8 (2009) 310–314.
[16] D.H. Ryan, J.M. Cadogan, C. Ritter, F. Canepa, A. Palenzona, M. Putti, Phys. Rev. B 80 (2009), 220503 (R).
[17] M. Pissas, D. Stamopoulos, Z.A. Ren, X.L. Shen, J. Yang, Z.X. Zhao, Supercond. Sci. Technol. 22 (2009) 055008.
[18] M.R. Cimberle, F. Canepa, M. Ferretti, A. Martinelli, A. Palenzona, A.S. Siri, C. Tarantini, M. Tropeano, C. Ferdeghini, J. Magn. Magn. Mater. 321 (2009) 3024–3030.
[19] J.D. Moore, et al., Supercond. Sci. Technol. 21 (2008) 092004.
[20] A. Yamamoto, et al., Appl. Phys. Lett. 92 (2008) 252501.
[21] A. Yamamoto A, et al., Supercond. Sci. Technol. 21 (2008) 095008.
[22] Y. Ding, Y. Sun, X.D. Wang, H.C. Wang, Z.X. Shi, Z.A. Ren, J. Yang, W. Lu, doi:10.1016/j.physc.2010.09.012.
[23] Z.A. Ren, et al., EPL 82 (2008) 57002, doi:10.1209/0295-5075/82/57002.
[24] D. Bhoi, P. Mandal, P. Choudhury, S. Dash, A. Banerjee, arXiv:1002.0208v1.
[25] W.G. Penney, R. Schlapp, Phys. Rev. 41 (1932) 194–207.
[26] V.P.S. Awana, R.S. Meena, A. Pal, K.V. Rao, H. Kishan, arXiv:1003.0273v1.
[27] L. Beaury, G. Calvarin, J. Derouet, J. Holsa, E. Sailynoja, J. Alloys Compd. 275–277 (1998) 646–650.
[28] J.W. Stout, L.M. Matarrese, Rev. Mod. Phys. 25 (1953) 338.
[29] G.K. Wertheim, D.N.E. Buchanan, Phys. Rev. 161 (1967) 478.
[30] M. Yuzuri, R. Tahara, Y. Nakamura, J. Phys. Soc. Japan 48 (1980) 1937.
[31] I.A. Santos, S. Gama, J. Appl. Phys. 86 (1999) 2334.
[32] F. Gomory, S. Takacs, Physica C 217 (1993) 297–312.
[33] C.Y. Lee, Y.H. Kao, Physica C 241 (1995) 167–180.
[34] M.J. Qin, X.X. Yao, Phys. Rev. B 54 (1996) 7536–7544.
[35] M. Polichetti, M.G. Adesso, D. Zola, J.L. Luo, G.F. Chen, Z. Li, N.L. Wang, C. Noce, S. Pace, Phys. Rev. B 78 (2008) 224523.
[36] P.J. Li, Z.H. Wang, A.M. Hu, Z. Bai, L. Qiu, J. Gao, Supercond. Sci. Technol. 19 (2006) 825–829.
[37] M.R. Koblischka, L. Pust, A. Galkin, P. Nalevka, Appl. Phys. Lett. 70 (1997) 514.
[38] K.–H. Muller, C. Andrikidis, Y.C. Guo, Phys. Rev. B 55 (1997) 630.

[39] M.R. Cimberle, C. Ferdeghini, R. Flukiger, E. Giannini, G. Grasso, D. Marre, M. Putti, A.S. Siri, Physica C 251 (1995) 61.
[40] M. Jirsa, V. Yurchenko, V. Novak, P. Kovac, I. Husek, Physica C 372–376 (2002) 1855–1858.
[41] M.R. Koblischka, L. Pust, A. Galkin, P. Nalevka, M. Jirsa, T.H. Johansen, H. Bratsberg, Phys. Rev. B 59 (1999) 12114.
[42] R.S. Gonnelli, D. Daghero, M. Tortello, G.A. Ummarino, V.A. Stepanov, R.K. Kremer, J.S. Kim, N.D. Zhigadlo, J. Karpinski, Physica C 469 (2009) 512–520.
[43] M.J. Qin, Z.X. Shi, H.L. Ji, X. Jin, X.X. Yao, H.C. Li, X.S. Rong, J. Appl. Phys. 78 (1995) 3287–3292.